jove

Label-Free Imaging of Lipid Storage Dynamics in *Caenorhabditis elegans* using Stimulated Raman Scattering Microscopy

Ayse Sena Mutlu[1], **Tao Chen**[1], **Dinghuan Deng**[1], **Meng C. Wang**[1,2,3]

[1] Huffington Center on Aging, Baylor College of Medicine [2] Department of Molecular and Human Genetics, Baylor College of Medicine [3] Howard Hughes Medical Institute, Baylor College of Medicine

Corresponding Author

Ayse Sena Mutlu
ozseker@bcm.edu

Citation

Mutlu, A.S., Chen, T., Deng, D., Wang, M.C. Label-Free Imaging of Lipid Storage Dynamics in *Caenorhabditis elegans* using Stimulated Raman Scattering Microscopy. *J. Vis. Exp.* (171), e61870, doi:10.3791/61870 (2021).

Date Published

May 28, 2021

DOI

10.3791/61870

URL

jove.com/video/61870

Abstract

Lipid metabolism is a fundamental physiological process necessary for cellular and organism health. Dysregulation of lipid metabolism often elicits obesity and many associated diseases including cardiovascular disorders, type II diabetes, and cancer. To advance the current understanding of lipid metabolic regulation, quantitative methods to precisely measure in vivo lipid storage levels in time and space have become increasingly important and useful. Traditional approaches to analyze lipid storage are semi-quantitative for microscopic assessment or lacking spatio-temporal information for biochemical measurement. Stimulated Raman scattering (SRS) microscopy is a label-free chemical imaging technology that enables rapid and quantitative detection of lipids in live cells with a subcellular resolution. As the contrast is exploited from intrinsic molecular vibrations, SRS microscopy also permits four-dimensional tracking of lipids in live animals. In the last decade, SRS microscopy has been widely used for small molecule imaging in biomedical research and overcome the major limitations of conventional fluorescent staining and lipid extraction methods. In the laboratory, we have combined SRS microscopy with the genetic and biochemical tools available to the powerful model organism, *Caenorhabditis elegans,* to investigate the distribution and heterogeneity of lipid droplets across different cells and tissues and ultimately to discover novel conserved signaling pathways that modulate lipid metabolism. Here, we present the working principles and the detailed setup of the SRS microscope and provide methods for its use in quantifying lipid storage at distinct developmental timepoints of wild-type and insulin signaling deficient mutant *C. elegans*.

Introduction

Obesity has become a global health problem threatening one third of the population around the world, and it presents a serious medical concern, given its association with poor mental health[1] and deadly diseases including diabetes[2], cardiovascular diseases[3] and some types of cancer[4]. Study of lipid metabolism is essential to better understand the biological problems behind obesity. Rapid and specific quantification of lipid storage entails the detection of fatty acids and their derivatives, as well as sterol-containing metabolites, with high sensitivity and preferably with spatial information. Lipids are challenging targets to image because they lack intrinsic fluorescence and cannot be easily fluorescently tagged. The fluorescent tags are often larger than the lipid molecules and, therefore, can be chemically invasive and impractical for in vivo applications. Label-free or minimal labeling strategy is necessary to preserve the hydrophobic structure of the lipid molecules[5]. Recent developments in imaging technologies have created exciting opportunities for label-free imaging of lipids in living cells, tissues, and organisms.

Traditional approaches for lipid storage analyses in biological samples include biochemical assays and staining protocols with lipophilic dyes. Biochemical quantification assays involving mass spectrometry (MS) are unmatched in their molecular resolvability, but they require very large sample amounts and sample preparation usually takes several hours, limiting their application for real-time imaging of living systems[5]. Another major limitation of these assays is the lack of spatial information. On the other hand, lipophilic dyes such as Oil Red O and Sudan Black provide tissue and cellular distribution of lipid storage organelles and compared to MS techniques, these staining methods are also low in cost and easy to perform. However, these staining protocols require fixation, which can impact the hydrophobic nature of the lipid droplets, generate artificial changes in their structure and result in inconsistencies between experiments[6]. The technical difficulties associated with biochemical and staining techniques have led to the search for label-free methods to image lipid molecules and to the rapid increase in the usage of coherent Raman scattering (CRS) microscopy in lipid imaging.

The Raman effect was first recognized by Raman and Krishnan, where they reported that upon interacting with a photon, a molecule can generate scattered light with no change in wavelength (called Rayleigh scattering) or rarely with an altered wavelength (called Raman scattering) and this change in wavelength is characteristic of the functional chemical groups within the molecule[7]. When the chemical bonds within a molecule get excited to a higher vibrational energy level by an incident photon, called pump photon, the energy of the scattered photon, called the Stokes photon, become lower. Otherwise, the chemical bonds can reach a lower vibrational energy level if they are originally at a higher level, and the scattered photon gain energy to be the anti-Stokes photon. The frequency difference between the incident and scattered photons is known as the Raman shift. Each chemical bond within a molecule has a characteristic and quantifiable Raman shift. For example, the CH_2 bond has a Raman shift of 2,845 cm^{-1}, which is abundant in fatty acid chains[8]. This spontaneous Raman signal is generally very weak, which has vastly limited the imaging speed in conventional spontaneous Raman microscopy. Over the years, various approaches have been developed to increase the imaging speed and sensitivity of spontaneous Raman microscopy. Coherent Raman scattering microscopy, including Coherent Anti-Stokes Raman Scattering (CARS) microscopy and Stimulated Raman Scattering (SRS) microscopy, is the most

recent progress. CARS and SRS have slightly different working principles, but both are label-free techniques that have live imaging capability, can yield spatial and temporal information on lipid storage dynamics, and only require small sample size. CARS microscopy suffers from non-resonant background, which comes from various non-linear processes, and CARS signals also have non-linear relationship with the molecule concentration, which together complicate the quantification process[9]. Unlike CARS microscopy, SRS microscopy does not generate non-resonant background signals and offers linear dependence on the concentration of the molecule of interest. Thus, currently SRS microscopy is more widely used for lipid imaging.

In SRS microscopy, the weak spontaneous Raman signals can be amplified when excited by two synchronized laser beams with their frequency difference matching the chemical bond vibrational frequency. The molecule will experience an enhanced transition to an excited state due to coherent excitation. As a result, the rate of Stokes photon generation is boosted. Consequently, the intensity of the transmitted "Stokes" beam increases (stimulated Raman gain, SRG) and the intensity of the transmitted "pump" beam decreases (stimulated Raman loss, SRL). Detection of SRG or SRL signals underlies the basis for Stimulated Raman Scattering (SRS) microscopy imaging of molecules with specific chemical bonds[10]. If the frequency difference between the two laser beams does not match the vibrational frequency of the chemical bond within a molecule of interest, neither SRG nor SRL signals will be generated. The imaging speed of SRS microscopy is around 2 µsec per pixel or 1 second per frame, which is much faster than spontaneous Raman microscopy[11]. Typical lateral resolution for SRS microscopy is diffraction limited and around 300 nm. In addition, the two-photon optical processes of SRS microscopy allow for volumetric 3D imaging of relative thick tissue samples and the imaging depth could reach 300–500 µm. Overall, SRS microscopy presents an efficient, label-free imaging technique to detect specific biomolecules, especially lipids.

Lipid droplets are single-membrane organelles, which are the main cellular storage site for neutral lipids, including the triacylglycerols (TAGs) and cholesterol esters (CEs). CH_2 bonds in the fatty acid chains of these lipid molecules generate strong SRS signals at 2,845 cm^{-1} when excited[8], thus enabling the detection and quantification of storage lipid levels in intact cells, tissue sections and even whole organisms[12,13,14,15]. In particular, *C. elegans* are useful for lipid imaging studies owing to their transparency. Like mammals, *C. elegans* also store lipids in lipid droplets and the synthesis and degradation pathways of lipid molecules are highly conserved[16]. In this protocol, we will provide the working principle of SRS microscopy, its fundamental setup and describe the methods for its use in lipid imaging in *C. elegans*.

Protocol

1. Instrumental setup for Stimulated Raman Scattering Microscopy

NOTE: The SRS microscopy system is built upon a picosecond laser with pump integrated optical parametric oscillator and a confocal laser scanning microscope. The oscillator provides two picosecond pulse trains, including a Stokes beam at 1,064 nm and a pump beam tunable between 700–990 nm. Temporal and spatial overlapping of the two beams are achieved inside the laser. A built-in electro-optic modulator (EOM) is designed specifically for SRS microscopy. This protocol will focus on coupling the laser with the microscope, and the daily operation of this

system (**Figure 1**). The configuration of an SRS microscope system is evolving in the last decade. It should be noted that the following description only represents one of the several configurations.

1. Feeding laser beams into the microscope
    1. Set up the periscope to lift the beam from picosecond light source exit to IR laser input port on the scanner of the microscope.
    CAUTION: Read the laser system manual before operation and take all required precautions because near infrared radiation generated by this Class IV laser system can cause severe harm to the eyes and skin. Complete the trainings that are required by the institutional environmental safety departments. Wear protective goggles and lab coat with cuffed sleeves.
    2. First, set the pump beam at 750 nm and lower down the laser power to 50 mW, which can be visually inspected, affiliating the alignment. Then, use a beam expander (**Figure 1**, L1 and L2) to adjust the beam diameter to fit the back aperture of microscope objectives. Use a two relay mirrors (**Figure 1**, M1 and M2) to guide the laser beam to the periscope (**Figure 1**, P1 and P2). The periscope will lift the beam to the height of the scanner opening and serve as the steering mirror for alignment as well.
    3. Set the knobs on the periscope at the center of the tuning range and choose the initial position and angle of each mirror such that the laser beam hits the center of the mirror, approximately.
    4. Perform the coarse alignment using an empty port on the objective turret and place the power meter probe to measure the power of the transmitted light. Set the scanner of the microscope at highest zoom (50x), and then measure the power of the transmitted light with the focused laser beam spot. Optimize the knobs on each mirror, M1 and M2, iteratively to achieve the highest transmitted laser power.
    5. Perform the fine alignment with the alignment tool. Put the fluorescence target alignment cap on the empty objective seat and adjust the knobs of M1 to center the spot. Then, introduce the extension tube for the target and tune the knobs of M2 to center the spot.
    6. Repeat steps 1.1.4 and 1.1.5 until the beam centers the target at both positions.
2. Connecting detection and electronics
    1. Set up the SRS detection module. Place a beam splitter cuber after the condenser to direct the transmitted laser to the photodiode module. The module includes a telescope to relay and change the beam size to fit the active area of the photodiode, as well as an optical filter to remove the modulated Stokes beam and let the pump beam go through for demodulation.
    2. Set up the electronics connection (**Figure 1**). The intensity of the Stokes beam is modulated by a built-in EOM at 20 MHz inside the picosecond tunable laser. The modulation frequency output from the laser is input into the lock-in amplifier as the reference frequency for demodulation. Feed the output signal of the photodiode into the lock-in amplifier for demodulating the SRL.
    NOTE: The one-box laser systems can be upgraded and thus their specifications can vary due to different

production date. The previous version of picosecond tunable laser system, used in this protocol, has a Stokes beam of 1,064 nm, but the recent version has a Stokes beam of 1,031 nm. The modulation frequency of EOM used in this protocol is customized to 8 MHz, but the default modulation frequency for the recent system can be 10 or 20 MHz.

3. Finally, feed the lock-in amplifier output into the analog box of the microscope to convert electrical analog signal to digital signal. The system should be ready to process the SRS signal.

3. Optimize imaging conditions

1. Make a chemical sample for system alignment. For example, use dodecane to optimize the microscope, because dodecane has a very strong SRS signal from the C-H bonds. Use a secure seal to make a mini chamber; put 5 µL of dodecane and cover it with a coverslip.

   NOTE: Replace the dodecane sample once it looks unclear or presents debris, with a new sample which could be used for alignment for 2–3 months.

2. Place the sample on the microscope stage. Properly focus on the liquid droplet. It can be done faster by looking for the edge of the dodecane pad. Adjust the condenser for Kohler illumination.

3. Set the imaging parameters. Check whether the delay stage is on the right numbers. Set the pump beam wavelength to 795.8 nm. Using an IR sensor card and IR viewer, check whether the pump beam path is still correct.

4. Set the power of the pump beam to 200 mW and the Stokes beam to 400 mW on the picosecond system control panel.

   NOTE: The laser throughputs from laser exit to post objective of the two beams are approximately 25% for pump and 14% for Stokes for this system setup. Therefore, a post objective power of pump beam is approximately 50 mW and for Stokes beam it is around 56 mW. The pulse width of the recent picosecond laser system has changed from 6 ps to 2 ps, therefore, the applied laser power should be even lower.

5. Set the lock-in amplifier gain to maximum. Open the shutter for both the beams, as well as the main shutter of the laser.

6. Scan the sample and check the image on the computer screen. Change the display mode into **Hi-Lo** in the imaging software. Adjust the range to see an ~50% saturation. Check whether the saturation is centered in the image. If not, carefully adjust the steering mirrors, M1 and M2, to maximize the image intensity and to center the peak intensity.

7. Fine tune the delay stage and find the maximum SRS signal intensity from the dodecane sample. The system is then ready for use.

2. Preparation of *C. elegans* samples for SRS microscopy imaging

NOTE: As model organisms, *Caenorhabditis elegans* have been proven to be very useful for multiple imaging techniques. They are whole-body transparent, therefore various tissues can be imaged in the intact animal without the need for dissection. In *C. elegans,* neutral lipids are stored in lipid droplets located in the intestine, which consists of 20 epithelial

cells located bisymmetrically around the intestinal lumen[16]. Hypodermal cells and oocytes also store lipids. The main form of storage lipids in *C. elegans* lipid droplets are the triacylglycerols (TAGs)[17], which generate strong SRS signals due to the abundance of CH_2 bonds present in their fatty acid chains. This section will focus on how to prepare *C. elegans* samples for SRS microscopy imaging and quantification of their total intestinal lipid storage levels.

1. Preparation of the imaging slides
    1. First, prepare 2% agarose solution in distilled H_2O, and make sure all the agarose melts before preparing the agarose pads.
    2. Add one drop of warm 2% agarose onto a blank slide (approximately 100 µL) that is placed between support slides with two layers of laboratory tape and quickly place a second slide on top of the first slide. Gently press to create a thin, even agarose pad.
    3. Set these slides aside in closed position and do not separate them until worms are ready to be mounted. Prepare fresh slides before each imaging session, as the pads will dry after 1 day.
    NOTE: Use multi-well imaging chambers, if imaging several worms in high-throughput genetic screens[18]. Use live imaging setups to image spatio-temporal dynamics of lipid metabolism through development and aging[19].
2. Mounting the worms
    1. Prepare the anaesthetizing agent by adding sodium azide or levamisole in M9 buffer to the final concentration of 100 mM or 1 mM, respectively.
    NOTE: Use levamisole if the worms need to be recovered after imaging for genotyping after genetic screens.
    CAUTION: Several anaesthetizing agents, including sodium azide and levamisole, are harmful if inhaled. Wear protective gloves and clothing, as well as use a chemical fume hood when preparing those working solutions.
    2. Place a drop of anaesthetizing agent to a coverslip (approximately 4–5 µL for 10–20 worms).
    NOTE: Adjust the amount of the anaesthetizing agent according to the worm number to keep the worms as close to each other as possible. Using too much liquid for few worms may cause the worms to spread on the agarose pad.
    3. Pick the worms to be imaged under the dissection microscopy and transfer them to the anaesthetizing agent droplet. After all the worms are added to the droplet, move them around using the worm picker and make sure they do not overlap with each other.
    4. Separate the glass slides (from step 2.1) without perturbing the agarose pad.
    5. Cover the worm droplet with the glass slide that has the agarose pad. Make sure the agarose pad is facing toward the worms. Alternatively, the anesthetizing aging droplet can also be added onto the agarose pad and worms can be covered with the coverslip.
    6. Finally, mark the location of the worms using a permanent marker on the glass slide.

3. Image acquisition and analysis

1. Acquiring the images using the SRS microscope system.

1. Before imaging any sample, determine the imaging parameters and verify SRS signals (as explained in Protocol 1).
2. Mount the slide with the coverslip facing the objective lens. Turn on the bright field light source and direct it to the eyepiece to locate the worms.
   NOTE: Use a 20x objective lens to image the lipid storage in the whole intestine. Consider using a 60x objective lens to image hypodermal fat storage or to quantify lipid droplet size/number.
3. Bring the worms into focus and adjust the condenser position accordingly.
4. Turn off the bright field light source and switch to the laser scanning unit. Begin scanning the first worm at a fast scanning rate (e.g., 512 x 512 pixels), and adjust the fine focus to find the area of interest. For the first sample to be imaged, adjust the laser powers to the level where SRS signals are not saturated.
5. Switch to a slower scanning rate (e.g., 2 µs/pixel) and higher resolution (e.g., 1024 x 1024 pixels) to obtain the SRS image.
   NOTE: Keep the laser powers constant for every sample to be imaged during the imaging session.
6. Save the SRS image in the desired format that enables high resolution (such as a .tiff file). Depending on the imaging software and setup used, save the location of the first worm before moving to the next.
7. Complete imaging of all worms that were mounted on the slide. Turn off the shutter to block the laser beams. Do not turn off the laser source until all samples are imaged.
8. Remove the slide before placing the next sample slide. Repeat steps 3.1.2–3.1.7.
9. Once all the samples have been imaged, put the laser source on standby and turn off the associated equipment including the amplifier, the detector, the microscope and the computer.

2. Analysis of images using ImageJ
   1. Open the image files (usually .tiff) to be quantified in ImageJ, by selecting the files and dragging and dropping them to the ImageJ window. Download the appropriate ImageJ plug-ins, if using specific Olympus microscope formats (such as .oib files).
   2. Select the properties to be analyzed (**Analyze** > **Set Measurements**). For total lipid storage quantitation, select **Area, Min and Max Gray Value,** and **Mean Gray value**.
   3. Use the polygon selection tool and outline the region of the worm intestine to be quantified. To measure the parameters selected in step 3.2.2, click on **Analyze** > **Measure**. A new window with the measurement results will pop-up. Repeat this step for all the open images.
   4. Select the measurements for all the worms in a given genotype and copy/paste the results to a new spreadsheet. Repeat the steps 3.2.1–3.2.4 for all the genotypes in the same imaging session.
   5. Select an area in the vicinity of the worm that does not have any SRS signal, to quantify as background. Make sure the area selected for background measurement does not contain any bacteria or debris that could also give an SRS signal.

6. Subtract the background mean gray value from the measurements of each individual worm. Calculate the average and standard deviation of the background subtracted mean gray values from all of the worms in a given genotype/test group. Normalize this value to the average of the control group.

7. Finally, perform the appropriate statistical analysis using the mean gray value as a measure for lipid levels in each worm. Typically, use Student's *t*-test for two groups and use one-way ANOVA with an appropriate multiple comparison test for more than two groups.

   NOTE: When selecting images for figure presentation, ensure that those selected images have the same pixel intensity distribution. Set the brightness and contrast to the same values for all the images in the same figure (**Image** > **Adjust** > **Brightness and Contrast**).

Representative Results

Insulin signaling is an important endocrine pathway that impacts development, reproduction, lifespan, and metabolism. In worms, insulin signaling consists of about 40 insulin-like peptide ligands, insulin-like growth factor receptor ortholog DAF-2, downstream PI3K/AKT kinase cascade, and the FoxO transcription factor ortholog, DAF-16[20]. *daf-2* mutants, that lack the insulin receptor, have more lipid droplets in their intestine, the worm lipid storage tissue[21,22]. Using SRS microscopy, we quantified the intestinal lipid levels in age-synchronized wild-type worms and *daf-2* mutants during adulthood. Consistent with the previous results, we found that *daf-2* mutants have higher lipid levels[23,24] (**Figure 2A**). We observed a decline in lipid levels in wild-type worms starting day 1 until day 9 of adulthood (**Figure 2A**). However, the lipid levels in *daf-2* mutants increased until they were 5-days-old and then they were constant around the level of 2.5–3.0 fold higher than the wild-type (**Figure 2A**).

DAF-16, the *C. elegans* FoxO transcription factor ortholog, orchestrates most of the downstream functions of the insulin signaling pathway. *daf-16* null mutations suppress several phenotypes observed in *daf-2* mutants, including fat accumulation. *daf-16* genomic locus encodes for 8 different transcripts (*daf-16a-h*), that are generated by either alternative transcription start site, or alternative splicing[20]. Among those, *daf-16a*, *daf-16b* and *daf-16d/f/h* are the most abundant transcripts and they encode for proteins with different N termini. Studies with isoform-specific mutations and transgenes suggested that DAF-16A and DAF-16D/F/H isoforms regulate dauer development and lifespan[24,25], whereas DAF-16B is important for pharyngeal remodeling during dauer formation[26]. In this study, using SRS microscopy, we investigated the isoform specificity of DAF-16 in regulating intestinal lipid storage. We found that *daf-16* inactivation suppresses the increase in lipid levels of *daf-2* mutants (**Figure 2B,C**). Expressing *daf-16a* or *daf-16b* isoform in the *daf-2; daf-16* double mutants does not restore the lipid levels. However, the expression of *daf-16d/f/h* isoform is sufficient to restore the lipid levels in *daf-2; daf-16* to the levels observed in *daf-2* single mutants (**Figure 2B,C**). These results revealed that specifically DAF-16D/F/H isoforms modulates lipid metabolism in *daf-2* mutant worms. This is also consistent with the results from a recent study that showed olfactory regulation of lipid storage is also mediated through the transcriptional activities of DAF-16D/F/H[27].

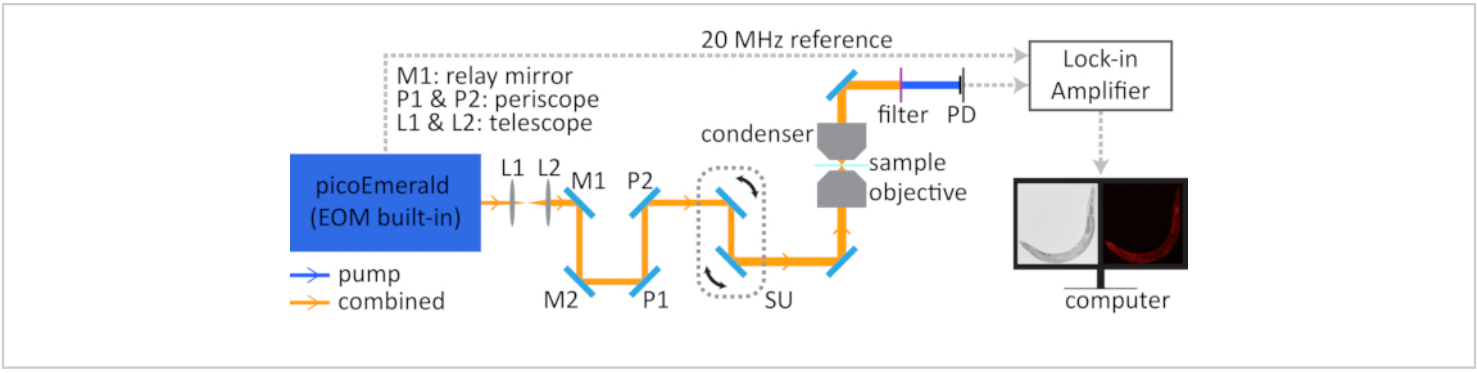

Figure 1: Illustration of the SRS microscope system. The all-in-one laser provides temporally and spatially combined pump and Stokes beams, built-in electro-optic modulator (EOM) and reference frequency for lock-in amplifier. The combined beam is expanded by the telescope (L1 and L2), relayed by two relay mirrors (M1 and M2) and lifted by the periscope (P1 and P2), and then sent into the scanner of the microscope. The combined beam is scanned by the scanning unit (SU) in the microscope and focused on the sample. Transmitted light is collected by the condenser. A filter will remove the Stokes beam and leave the pump beam to be detected by the photodiode (PD). The gray dashed arrows show the connection between the electronics. Please click here to view a larger version of this figure.

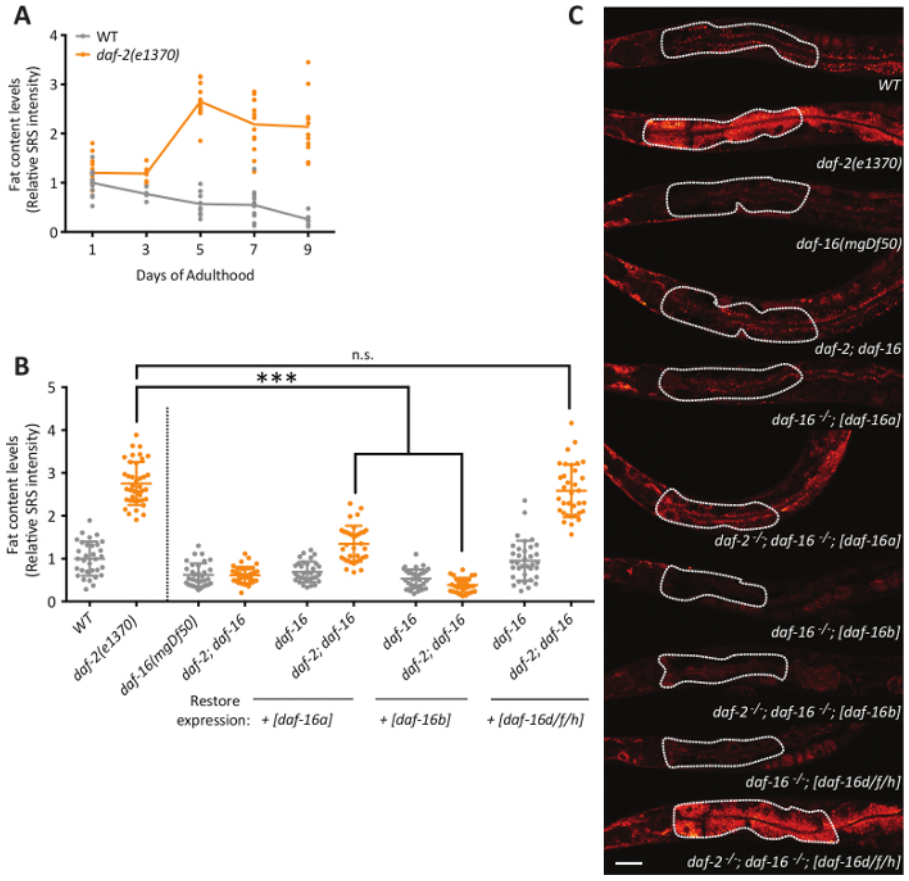

Figure 2: Reduced insulin signaling in *C. elegans* leads to increased lipid storage. (**A**) Using SRS microscopy, intestinal lipid levels of wild-type and *daf-2* mutants worms are quantified in day 1, 3, 5, 7 and 9 of adulthood. In wild-type worms, the lipid levels decline over time, whereas *daf-2* mutants accumulate lipids until day 5 and they have about 2.7 fold more lipids compared to wild-type worms. (**B**) *daf-16* deletion suppresses the increased lipid levels in *daf-2* mutants. Restoring expression of the *daf-16d/f/h* isoform in *daf-2; daf-16* double mutants is sufficient to increase lipid levels to *daf-2* mutants' levels, whereas restoring expression of *daf-16a* or *daf-16b* isoforms is not. *** $p < 0.001$, n.s. not significant by one-way ANOVA with Bonferroni's multiple comparisons test. (**C**) Representative SRS images. Yellow pixels indicate higher lipid levels. Quantified intestinal area is shown in dashed lines. Scale bar is 40 µm. Please click here to view a larger version of this figure.

Supplementary File. Please click here to download this File.

Discussion

In defense against obesity and its associated metabolic disorders, important research efforts have been implemented to better understand the regulatory mechanisms of lipid homeostasis. For quantitative detection of lipid molecules in biological samples, label-free imaging by SRS microscopy has been proven to be a reliable alternative to biochemical assays and other staining methods. Our group and others

have revealed novel biological mechanisms in lipid metabolic regulation by combining the use of *C. elegans* and SRS microscopy[12,18,28,29,30,31]. In this protocol, using SRS microscopy we demonstrated that downregulating insulin signaling in worms leads to an increase in total intestinal lipid levels. We observed that starting day 1 of adulthood, lipids accumulate in the intestine of the *daf-2* mutants, which have loss-of-function mutation in the insulin receptor gene, whereas in wild-type worms intestinal lipid levels decline. Additionally, consistent with previous studies[23,24], we found that *daf-16* inactivation can fully suppress the lipid storage increase in *daf-2* mutants and among the different *daf-16* isoforms, *daf-16d/f/h* isoform specifically regulates lipid homeostasis. As previous studies suggested, the difference in total intestinal lipid storage levels in *daf-2* mutants is likely due to a combination of factors: increased *de novo* lipid synthesis[32], decreased lipid utilization[33], as well as reduced reproduction, and yolk accumulation[34]. Recent advances in coherent Raman spectroscopy techniques (SRS and CARS) would help further elucidate the mechanisms of how insulin signaling contributes to the regulation of different lipid storage types in distinct tissues, including the intestine, hypodermis and oocytes.

SRS microscopy has been utilized to image not only lipids, but also other biomolecules, including DNA[35], RNA[14], proteins[13], and glucose[36]. It has been implemented to provide important insights into many aspects of biology such as cell biology, microbiology, cancer biology, and developmental biology[11]. More recently, the use of bioorthogonal tags (e.g., alkyne and deuterium tags), to minimally label the molecules of interest, further enhanced the detection sensitivity and specificity. These minimal vibrational tags do not disrupt the chemical properties of the molecule, but provide specific chemical contrast, as their Raman signal is within the “silent window” of the Raman spectrum[14,37]. In addition to improving sensitivity and specificity, achieving super-resolution SRS imaging is also an exciting area of research. Several research groups also have efforts in minimizing the equipment size by creating hand-held SRS microscope[38]. Thus, application of SRS imaging to biomedical research has opened up new venues for technological and chemical improvements to advance lipid imaging.

Compared to traditional methods of lipid quantitation, SRS microscopy has several advantages. First of all, it is performed in a label-free manner and even if a label has to be used, the label can be as small as two atoms. Therefore, it also does not suffer from the photobleaching problem as other fluorescent tagging and staining methods. Secondly, the capability of live imaging using whole organisms enables tracking the dynamics of specific metabolites[29,39,40]. Finally, SRS microscopy permits higher degree of multiplexing and therefore can be implemented to image multiple biomolecules in distinct cellular compartments simultaneously. Hyperspectral SRS/CARS microscopy holds great future in exploring the metabolic dynamics of several distinct biomolecules, as well as different types of lipid storage compartments such as yolk particles in *C. elegans*[41] or cholesteryl ester and TAG rich lipid droplets in different mammalian cells and tissues[31]. On the other hand, SRS microscopy is facing limitations such as high cost in hardware and lack of full commercial availability. Additionally, it requires expertise to maintain and run the system, which can complicate its adoption. The developments in light source and system integration are improving the situation. Fiber-based low cost laser source and fully integrated systems offer new opportunities in commercialization and will help reduce the

cost in the future[11,42,43]. In addition, despite the new technological approaches to improve the imaging speed and spatial resolution of SRS imaging, the limited detection sensitivity may continue to hinder the capability to probe metabolites of low abundance. Overall, the use of SRS microscopy in biomedical research has grown tremendously in the last decade. SRS imaging will further benefit from the technological improvements in detection sensitivity, spatial resolution and multiplexing capability, and ultimately expand its use in quantitative monitoring of biomolecules, especially lipids.

Disclosures

The authors have nothing to disclose.

Acknowledgments

This work was supported by NIH grants R01AG045183 (M.C.W.), R01AT009050 (M.C.W.), R01AG062257 (M.C.W.), DP1DK113644 (M.C.W.), March of Dimes Foundation (M.C.W.), Welch Foundation (M.C.W.), and by HHMI investigator (M.C.W.). We thank the Caenorhabditis Genetics Center (CGC) for *C. elegans* strains.

References

1. Luppino, F. S. et al. Overweight, obesity, and depression: a systematic review and meta-analysis of longitudinal studies. *Archives of General Psychiatry.* **67** (3), 220-229 (2010).
2. Eckel, R. H. et al. Obesity and type 2 diabetes: what can be unified and what needs to be individualized? *Diabetes Care.* **34** (6), 1424-1430 (2011).
3. Poirier, P. et al. Obesity and cardiovascular disease: pathophysiology, evaluation, and effect of weight loss. *Arteriosclerosis, Thrombosis, and Vascular Biology.* **26** (5), 968-976 (2006).
4. Bhaskaran, K. et al. Body-mass index and risk of 22 specific cancers: a population-based cohort study of 5.24 million UK adults. *Lancet.* **384** (9945), 755-765 (2014).
5. Shen, Y., Hu, F., Min, W. Raman imaging of small biomolecules. *Annual Review of Biophysics.* **48**, 347-369 (2019).
6. Daemen, S., van Zandvoort, M., Parekh, S. H., Hesselink, M. K. C. Microscopy tools for the investigation of intracellular lipid storage and dynamics. *Molecular Metabolism.* **5** (3), 153-163 (2016).
7. Syed, A., Smith, E. A. Raman imaging in cell membranes, lipid-rich organelles, and lipid bilayers. *Annual Review of Analytical Chemistry (Palo Alto, Calif.).* **10** (1), 271-291 (2017).
8. Thomas, G. J., Jr. Raman spectroscopy of protein and nucleic acid assemblies. *Annual Review of Biophysics and Biomolecular Structure.* **28**, 1-27 (1999).
9. Evans, C. L., Xie, X. S. Coherent anti-stokes Raman scattering microscopy: chemical imaging for biology and medicine. *Annual Review of Analytical Chemistry (Palo Alto, Calif.).* **1**, 883-909 (2008).
10. Freudiger, C. W. et al. Label-free biomedical imaging with high sensitivity by stimulated Raman scattering microscopy. *Science.* **322** (5909), 1857-1861 (2008).
11. Hu, F., Shi, L., Min, W. Biological imaging of chemical bonds by stimulated Raman scattering microscopy. *Nature Methods.* **16** (9), 830-842 (2019).
12. Wang, M. C., Min, W., Freudiger, C. W., Ruvkun, G., Xie, X. S. RNAi screening for fat regulatory genes with SRS microscopy. *Nature Methods.* **8** (2), 135-138 (2011).

13. Wei, L., Yu, Y., Shen, Y., Wang, M. C., Min, W. Vibrational imaging of newly synthesized proteins in live cells by stimulated Raman scattering microscopy. *Proceedings of the National Academy of Sciences of the United States of America.* **110** (28), 11226-11231 (2013).
14. Wei, L. et al. Live-cell imaging of alkyne-tagged small biomolecules by stimulated Raman scattering. *Nature Methods.* **11** (4), 410-412 (2014).
15. Ramachandran, P. V., Mutlu, A. S., Wang, M. C. Label-free biomedical imaging of lipids by stimulated Raman scattering microscopy. *Current Protocols in Molecular Biology.* **109**, 30 33 31-30 33 17 (2015).
16. Srinivasan, S. Regulation of body fat in Caenorhabditis elegans. *Annual Review of Physiology.* **77**, 161-178 (2015).
17. Vrablik, T. L., Petyuk, V. A., Larson, E. M., Smith, R. D., Watts, J. L. Lipidomic and proteomic analysis of Caenorhabditis elegans lipid droplets and identification of ACS-4 as a lipid droplet-associated protein. *Biochimca Et Biophysica Acta.* **1851** (10), 1337-1345 (2015).
18. Yu, Y., Mutlu, A. S., Liu, H., Wang, M. C. High-throughput screens using photo-highlighting discover BMP signaling in mitochondrial lipid oxidation. *Nature Communications.* **8** (1), 865 (2017).
19. Kelley, L. C. et al. Live-cell confocal microscopy and quantitative 4D image analysis of anchor-cell invasion through the basement membrane in Caenorhabditis elegans. *Nature Protocols.* **12** (10), 2081-2096 (2017).
20. Murphy, C. T., Hu, P. J. Insulin/insulin-like growth factor signaling in C. elegans. *WormBook.* 1-43 (2013).
21. Shi, X. et al. Regulation of lipid droplet size and phospholipid composition by stearoyl-CoA desaturase. *Journal of Lipid Research.* **54** (9), 2504-2514 (2013).
22. Watts, J. L., Ristow, M. Lipid and carbohydrate metabolism in Caenorhabditis elegans. *Genetics.* **207** (2), 413-446 (2017).
23. Kimura, K. D., Tissenbaum, H. A., Liu, Y., Ruvkun, G. daf-2, an insulin receptor-like gene that regulates longevity and diapause in Caenorhabditis elegans. *Science.* **277** (5328), 942-946 (1997).
24. Kwon, E. S., Narasimhan, S. D., Yen, K., Tissenbaum, H. A. A new DAF-16 isoform regulates longevity. *Nature.* **466** (7305), 498-502 (2010).
25. Chen, A. T. et al. Longevity genes revealed by integrative analysis of isoform-specific daf-16/FoxO mutants of Caenorhabditis elegans. *Genetics.* **201** (2), 613-629 (2015).
26. Lee, R. Y., Hench, J., Ruvkun, G. Regulation of C. elegans DAF-16 and its human ortholog FKHRL1 by the daf-2 insulin-like signaling pathway. *Current Biology.* **11** (24), 1950-1957 (2001).
27. Mutlu, A. S., Gao, S. M., Zhang, H., Wang, M. C. Olfactory specificity regulates lipid metabolism through neuroendocrine signaling in Caenorhabditis elegans. *Nature Communications.* **11** (1), 1450 (2020).
28. Chen, A. J. et al. Fingerprint Stimulated Raman Scattering imaging reveals retinoid coupling lipid metabolism and survival. *Chemphyschem: a European Journal of Chemical Physics and Physical Chemistry.* **19** (19), 2500-2506 (2018).
29. Li, X. et al. Quantitative imaging of lipid synthesis and lipolysis dynamics in Caenorhabditis elegans by

Stimulated Raman Scattering microscopy. *Analytical Chemistry.* **91** (3), 2279-2287 (2019).

30. Lin, C. J., Wang, M. C. Microbial metabolites regulate host lipid metabolism through NR5A-Hedgehog signalling. *Nature Cell Biology.* **19** (5), 550-557 (2017).
31. Fu, D. et al. In vivo metabolic fingerprinting of neutral lipids with hyperspectral stimulated Raman scattering microscopy. *Journal of the American Chemical Society.* **136** (24), 8820-8828 (2014).
32. Perez, C. L., Van Gilst, M. R. A 13C isotope labeling strategy reveals the influence of insulin signaling on lipogenesis in C. elegans. *Cell Metabolism.* **8** (3), 266-274 (2008).
33. Elle, I. C., Rodkaer, S. V., Fredens, J., Faergeman, N. J. A method for measuring fatty acid oxidation in C. elegans. *Worm.* **1** (1), 26-30 (2012).
34. Ezcurra, M. et al. C. elegans eats its own intestine to make yolk leading to multiple senescent pathologies. *Current Biology.* **28** (16), 2544-2556 e2545 (2018).
35. Lu, F. K. et al. Label-free DNA imaging in vivo with stimulated Raman scattering microscopy. *Proceedings of the National Academy of Sciences of the United States of America.* **112** (37), 11624-11629 (2015).
36. Long, R. et al. Two-color vibrational imaging of glucose metabolism using stimulated Raman scattering. *Chemical Communications (Cambridge, England).* **54** (2), 152-155 (2018).
37. Zhao, Z., Shen, Y., Hu, F., Min, W. Applications of vibrational tags in biological imaging by Raman microscopy. *Analyst.* **142** (21), 4018-4029 (2017).
38. Liao, C. S. et al. In vivo and in situ spectroscopic imaging by a handheld Stimulated Raman Scattering Microscope. *ACS Photonics.* **5** (3), 947-954 (2018).
39. Lee, H. J. et al. Assessing cholesterol storage in live cells and C. elegans by stimulated Raman scattering imaging of phenyl-Diyne cholesterol. *Scientific Reports.* **5**, 7930 (2015).
40. Wang, P. et al. Imaging lipid metabolism in live Caenorhabditis elegans using fingerprint vibrations. *Angewandte Chemie (International Edition in English).* **53** (44), 11787-11792 (2014).
41. Chen, W. W. et al. Spectroscopic coherent Raman imaging of Caenorhabditis elegans reveals lipid particle diversity. *Nature Chemical Biology.* **16** (10), 1087-1095 (2020).
42. Freudiger, C. W. et al. Stimulated Raman Scattering microscopy with a robust fibre laser source. *Nature Photonics.* **8** (2), 153-159 (2014).
43. Brinkmann, M. et al. Portable all-fiber dual-output widely tunable light source for coherent Raman imaging. *Biomedical Optics Express.* **10** (9), 4437-4449 (2019).